INSTITUTE OF PHYSICS PUBLISHING MEASUREMENT SCIENCE AND TECHNOLOGY

Meas. Sci. Technol. **16** (2005) 2121–2128 doi:10.1088/0957-0233/16/11/001

Nanometre resolution metrology with the Molecular Measuring Machine

John A Kramar

National Institute of Standards and Technology, Gaithersburg, MD 20899, USA

Received 18 March 2005, in final form 2 June 2005
Published 23 September 2005
Online at stacks.iop.org/MST/16/2121

Abstract

Nanometre accuracy and resolution metrology over technically relevant areas is becoming a necessity for the progress of nanomanufacturing. At the National Institute of Standards and Technology, we are developing the Molecular Measuring Machine, a scanned probe microscope (SPM) and Michelson interferometer based metrology instrument, designed to achieve nanometre measurement uncertainty for point-to-point measurements over a 50 mm by 50 mm working area. The salient design features are described, along with example measurements that demonstrate the measurement capabilities so far achieved. Both long-range measurements of sub-micrometre pitch gratings over 10 mm, and short-range, high-resolution measurements of a molecular crystal lattice have been accomplished. The estimated relative measurement uncertainty so far attained for pitch measurements is 6×10^{-5}, coverage factor $k = 2$. We have also used this instrument and scanning probe oxidation lithography for creating some simple nanometre dimension patterns that could serve as prototype calibration standards, utilizing the SPM probe tip positioning accuracy.

Keywords: nanometrology, STM, Michelson interferometer, grating, calibration, vacuum

(Some figures in this article are in colour only in the electronic version)

1. Introduction

Interest abounds and much hope has been placed in the current explosion of research efforts in nanotechnology and nanomanufacturing. Incredible devices have been proposed in fields as diverse as medicine, information technology and military applications. Several novel devices have been demonstrated in prototype form or limited initial production, for example artificial noses [1], molecular electronics memory and logic elements [2] and biological probes and medical diagnostics and therapeutics [3]. For these impressive early ideas and successes to mature into a widespread, stable and profitable economic sector requires that the infrastructural base of dimensional metrology be extended into this nanoscopic regime [4]. Mass production requires process control, and this requires accurate metrology. Metrology is also needed in any commerce or trade for quality assurance and communication of specifications and capabilities.

It is with this growing need in view that the National Institute of Standard and Technology has undertaken the task of extending as far as possible into the nanometre region the diverse dimensional metrology techniques available, including optical microscopy, scanning electron microscopy and scanning probe microscopy (SPM). Each of these is preferable for certain metrology tasks as one balances the competing requirements of resolution, accuracy, throughput, ambient environment and cost. For SPM, a key metrology instrument we are developing is the Molecular Measuring Machine (M^3) [5–7]. M^3 is an SPM-based metrology instrument that is designed to achieve sub-nanometre resolution with its probe and metrology system, over a macroscopic area of 50 mm by 50 mm. The goal is to achieve 1 nm combined uncertainty for point-to-point measurements within the working area.

Because of the recognized importance of developing the measurement infrastructure for nanotechnology, many national metrology institutes worldwide have similar ongoing efforts in the development of SPM-based metrology instruments [8–13]. The metrological performance of various SPMs has been compared by Breil *et al* [14]. This study included both standard and special metrological SPMs, and

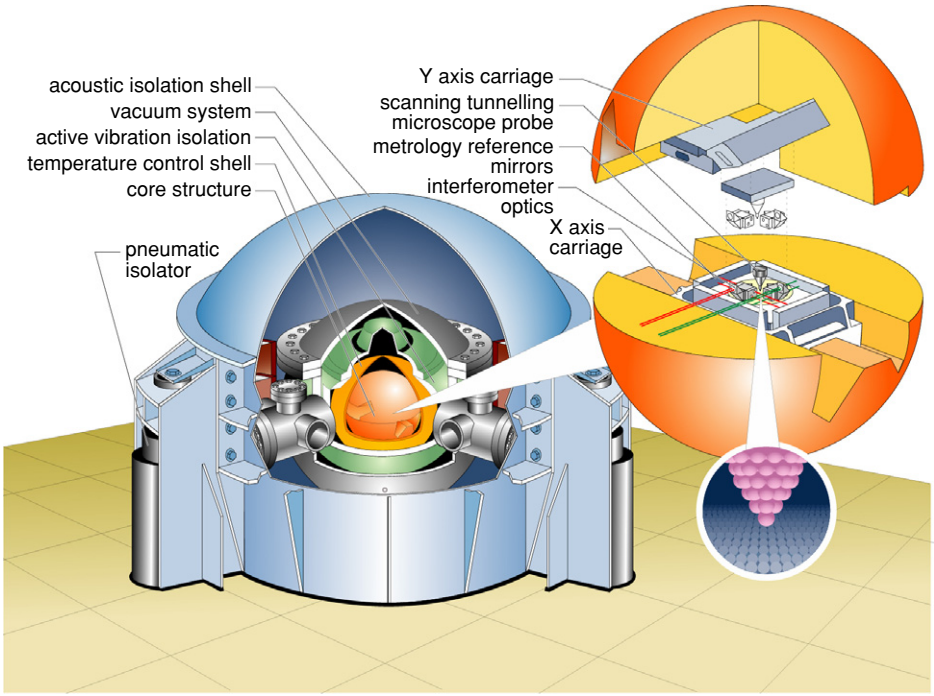

Figure 1. Cut-away view of the Molecular Measuring Machine.

clearly showed the need for active metrology sensors to achieve the necessary measurement accuracy. In general, all of these instruments operate over sub-millimetre ranges; however, there are a few large range (25 mm or greater) interferometer-based SPM metrology instruments and stages that have also been developed [15–17].

In this paper, we will describe some of the salient design features of the NIST Molecular Measuring Machine that enable the achievement of the uncertainty goal over the large range. Then we will present some example measurements that demonstrate the level of performance so far possible. These include long-distance measurements of line gratings and high-resolution measurements of a molecular crystal lattice. M^3 can also be used to create features on substrates using SPM lithography techniques, and some examples of prototype calibration artefacts created with M^3 will be shown.

2. M^3 design

To achieve sub-nanometre-scale metrology over centimetre-scale areas, a specialized instrument design is required. Key design requirements that must be accentuated because of the large range-over-resolution goal are vibration isolation, machine stiffness and low noise in the control electronics, which together are needed to minimize the positional noise. For measurement accuracy, care must also be taken to design for motion accuracy and repeatability, and high-stability temperature control to minimize measurement uncertainty due to thermal expansion effects. In addition, we have chosen to operate in a vacuum environment, both to reduce sample contamination and adsorbed overlayers, and to remove measurement errors in the interferometers due to changes in the refractive index of the ambient air.

For the basic machine core structure, a spherical geometry was chosen to maximize stiffness and symmetry, which also gives improved thermal uniformity and stability. The core is 350 mm in diameter, made out of pure copper, again for thermal uniformity and for long-term creep stability.

The planar motion is generated separately as one-dimensional (1D) motions of the sample relative to the core (X-axis carriage), and orthogonally, of the probe relative to the core (Y-axis carriage) (figure 1, inset). Avoiding stacked stages avoids position-dependent cross-talk between the axes, simplifying the error mapping of the planar motion into two 1D maps. To achieve the desired range over resolution, each axis of motion is a combination of a coarse motion and fine motion stage. Here stacked stages are used, but the small range of the fine motion stage, and the resulting limited mass shift, is small enough that the effect on the attitude of the coarse motion stage should be negligible. For repeatability, the coarse motion stages are guided by slideways. The motion is generated by linear piezoceramic stepper motors, from which sub-micrometre position control is readily achieved over the 50 mm linear range. The piezoceramic motors also have a decided advantage over electromagnetic stepper motors in terms of minimal heat generation. The fine motion stages are guided by parallel flexure elements and have a range of about 10 μm. They are driven directly by piezoceramics, with any parasitic lateral drive motion somewhat decoupled by means of a flexible coupling element. The fine stage resolution is limited only by the noise on the control electronics and high-voltage amplifiers, and for highest resolution work, the noise can be scaled down by scaling down the motion range.

For metrology purposes, the relative motion of the upper and lower fine motion stages, carrying the probe and sample respectively, is measured using a 2D displacement measuring interferometer system (figure 2). The interferometers measure

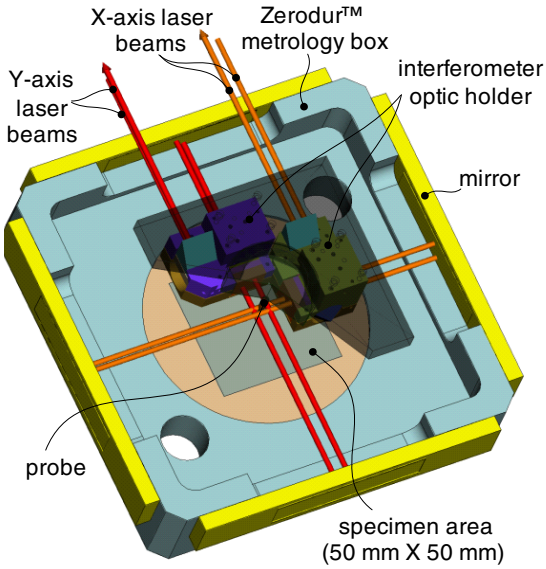

Figure 2. Differential interferometer beam path view. The position of the central assembly is measured with respect to the metrology box. The input and output beams are directed along the motion axis of the central assembly.

differentially the combined motion of the coarse and fine stages, giving a continuous metric independent of what portion of the total motion was generated by the fine or coarse stages. (For error mapping, the position of each fine motion stage is also measured relative to its coarse motion stage, using a capacitance gauge.) The reference mirrors for the interferometer are the inside surfaces of a highly accurate, low-expansion-coefficient metrology box, inside of which lies the sample. The interferometer beam-splitter optic assemblies are carried by the upper carriage on the same mounting plate that carries the probe system, suspended inside the metrology box. With this inside, differential optical configuration, Abbe offset is unavoidable—in our case it is roughly 10 mm. It follows that the parasitic angular motions of the carriages must be constrained to be well below 10^{-7} radians (or measured and corrected at this level) to achieve our design goal of 1 nm measurement uncertainty. This is a daunting challenge. Still, this interferometer configuration does in principle have some compensatory aspects (e.g., in the realm of minimizing the thermal sensitivity), and is conceptually a much simpler arrangement than the alternatives, given the need to measure the relative motion of two independent stages that are both moving relative to the laboratory frame.

A scanning probe microscope is used as the sample imaging probe system for M^3. It was, in fact, the advent of atomic-resolution imaging using scanning tunnelling microscopy (STM) that inspired the project from the beginning, as an attempt to achieve this same level of metrological resolution and uncertainty over as large an area as possible. The probe system is comprised of coarse and fine motion stages, a capacitance gauge position sensor, and the probe itself (figure 3). It was in-house designed to meet the various constraints, notable among them the very limited available space. The coarse motion stage is a cylindrical piezoceramic linear stepper motor that operates in the vertical axis with a 3 mm range. The grounded or open circuit clamping force is sufficient to keep the motor slug from sliding down when the power is removed. Built into this motor slug is the vertical, 5 μm range fine motion stage, having flexure-guided motion, and driven by a piezoceramic through a decoupling mechanism of a ball between two flats. The elements of the fine motion stage had to be folded back through the coarse motion stage to accommodate the space constraints. There is no horizontal (scan) motion built into the probe system, because any such motion would not be measured by the interferometer system; all horizontal scanning either drives the metrology box containing the sample or drives the entire upper assembly that includes the probe system along with the interferometer optics, as already described. The vertical fine motion is measured relative to the vertical coarse motion stage using a capacitance gauge that is calibrated *ex situ* against an interferometer. For a given measurement, the vertical range is limited to that provided by the guided fine motion stage. The vertical coarse motion is only crudely guided by the cylindrical housing in which the motor slug runs, and is not considered to be sufficiently characterized or repeatable to use during measurements, since it is within the metrology loop.

The example measurements in this paper were all done using an STM probe, which is simply a sharpened metal tip carried by the described vertical motion system. We are now in the process of developing an atomic force microscope probe which can also be used with the M^3 stages. Once again, one of the major obstacles to using commercial equipment was the

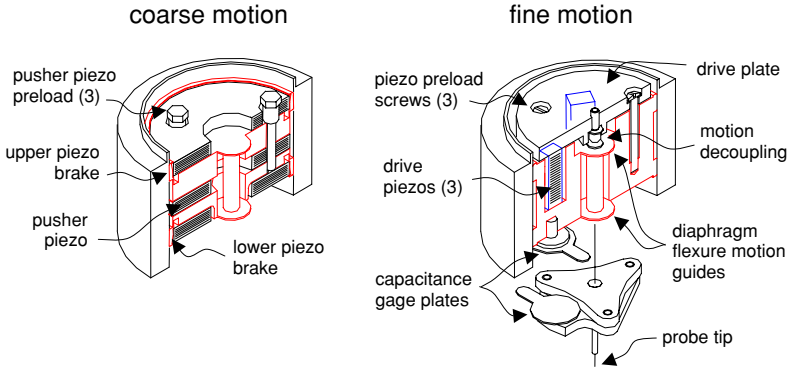

Figure 3. Probe actuator assembly exploded views, showing separately the detail of the coarse and fine motion mechanisms. The coarse motion is a linear piezo stepping motor. The fine motion is a folded, piezo-driven, flexure-guided system, with a capacitance gauge sensor.

space limitation; another constraint was our desire to maintain vacuum operation. We also wished to have an electrically conductive probe tip, with some flexibility as to material and dimension. This way, with the same probe assembly, we can switch between tunnelling current and force as the servo signal, or use force to servo while using the conductive tip for probing surface electronic properties or for applying a bias for surface modification. The AFM probe that we are developing is based on a vibrating tuning fork sensor [18]; the tips to date have been made from 25 μm diameter W or Cu wire, glued or soldered in place and electrochemically etched to a point.

Contained on the mounting plate, along with the interferometer optics and the probe system, are a pre-amplifier for measuring the tunnelling current, and a small video camera for coarse positioning of the probe tip over the feature or region of interest.

The machine core assembly is enclosed in layers of environmental isolation and control, as illustrated in figure 1. The first layer is a temperature control shell. This is a gold-coated copper sphere about 50 mm larger in diameter than the machine core, spiral-wrapped with polyimide-insulated copper wire at a 6 mm spacing. The shell has three doors on rails to allow the removal and replacement of the coarse motion carriages. To maintain a stable temperature at 20 °C, the room is kept at 17 °C ± 0.01 °C, and the current through the heater shell wire is controlled. There are several thermocouples distributed about the temperature control shell and the machine core to monitor the temperature, as well as platinum resistance thermometers on the probe mounting plate and near the sample. The control scheme is to maintain stability through thermal inertia and by keeping a constant heat load. Between the large thermal mass of the copper core and the weak coupling between it and the temperature control shell, the temperature rise time for the system is on the order of one day. Temperature stability of ±1 m°C has been demonstrated.

The next layer of environmental control is an active vibration isolation system. For this, the payload is suspended inside an outer shell, kinematically constrained by means of six actuator rods in the Mallock [19] suspension configuration, each actuator having an accompanying accelerometer mounted as nearly as possible coaxially, on the suspended inner mass. Different vibration compensation control algorithms have been implemented using a digital signal processor (DSP) [20], which have good effect when the vibration environment is noisy, for example when the turbomolecular pump is operating. In the quieter environment in which we more typically operate, the performance of the active system is limited by the sensor noise, and is less useful.

The entire instrument described to this point is contained in a vacuum system equipped with a turbo pump for roughing and eight symmetrically placed ion pumps for quiet operation. Several of the machine components will not withstand the bake out temperatures needed to achieve ultra-high vacuum levels; a typical base pressure reached is 10^{-5} Pa. The vacuum system is contained in an environmental control chamber that can be hermetically sealed to provide further acoustic isolation. This chamber is supported by pneumatic isolators having level control and a damped natural resonance of about 1 Hz.

We have recently moved this instrument to our new Advanced Metrology Laboratory [21]. The new laboratory space is in a building that is completely underground. The laboratory is a class 100 clean room with ±0.01 °C temperature control, and yet is acoustically quiet. The instrument rests on a pneumatically supported concrete slab that is in a pit under the walk-on floor. Most of the electronics and power supplies that drive the instrument are located in an adjacent control room.

The control system for M^3 runs on multiple DSPs on a VME (Versa Module Europa) backplane. The VME processor cards each have mezzanine input/output boards for reading from and controlling the instrument. The overall system control is done from a desktop computer that communicates with the VME through a bus adaptor. Code for the DSPs is developed on the desktop computer. User interface and top-level control is done in the Matlab[1] programming environment on the desktop computer.

3. Measurement examples

An ultimate performance goal for M^3 is to be able to repeatably locate any specific atom within the 50 mm by 50 mm measurement area, and measure the distance between it and any other atom. Naturally, this would also require a highly optimized sample artefact. Short of that, we present here measurement examples that separately demonstrate long-range and high-resolution operation.

3.1. Long distance

The first type of artefact that was measured by M^3 to validate the long-distance measurement operation was a laser-focused atomic-deposition (LFAD) Cr grating [22]. These gratings are produced by depositing neutral Cr atoms onto a suitable substrate (in this case a Si wafer chip) through a standing wave of high-intensity laser radiation, tuned near an atomic transition. The induced dipole interaction causes the atoms to be focused to the nodes or anti-nodes, depending on the sign of the detuning. The expected value of the pitch is (212.77 ± 0.01) nm, which has also been validated by comparison with diffraction measurements. (All uncertainties are reported with a coverage factor $k = 2$, essentially two standard deviations.)

To measure the average pitch of this sample with the lowest uncertainty possible, we measured a section of the grating extending for 1 mm; this was approximately the maximum size of the gratings in this dimension. Measuring over a long distance and dividing by the number of line spacings minimizes the effect of line-location-determination uncertainty, or more generally, end-point uncertainty. The data were acquired by measuring individual 5 μm by 6 μm images using the fine motion carriages (figure 4). Two hundred images overlapping each other by 1 μm were acquired under continuous automated operation over a period of a week by sequentially positioning the coarse motion carriages. At the end of this measurement, the starting point image was re-measured to assess any shift in the probe tip location relative to the interferometer optics that might have occurred during the

[1] Certain commercial products are identified in this document for clarity and specificity. Such identification does not imply recommendation or endorsement by the National Institute of Standards and Technology, nor does it imply that the products identified are necessarily the best available for the purpose.

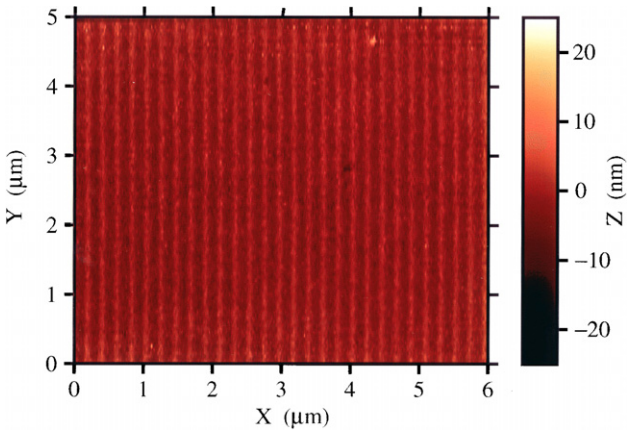

Figure 4. Single M^3 metrology image of LFAD Cr grating, acquired under closed-loop, interferometer-measured, position control in the *X* and *Y* directions.

course of the measurement due to, e.g., inadvertent tip–sample contact, or material creep. Additional spot checks were also made along the length of the overall measurement.

Since the interferometers measure the combined motion of the coarse and fine carriages, there is fundamentally no stitching error or ambiguity in combining the individual images into a complete image or data set. At a more detailed level, some level of correction to the pixel locations is necessary due to stage motion cross coupling. This is due to the motion coupling from the horizontal fine motion stages into the vertical axis, in combination with the coupling of the vertical fine motion stage into the horizontal axes; this latter coupling is inside the metrology loop, and is not measured. Either of these parasitic motions alone would be insufficient to generate a position error, as long as the sample surface were well aligned with the coarse motion plane. Happily, this error is non-cumulative between individual images, and the accuracy of the correction factor within the images can be verified by observing the overlapping regions. More difficult to assess and correct is the Abbe error. For this grating measurement, no Abbe correction was attempted; instead, the uncertainty due to this effect was estimated based on the magnitude of the Abbe offset and the previously measured magnitude of the pitch and roll of the coarse motion carriages during translation. A listing of the sources of uncertainty and their magnitude is given in [6]. The average pitch of the grating was calculated by taking the distance and estimated measurement uncertainty between two lines a full millimetre apart, and dividing by the counted number of line spacings between them, yielding (212.69 ± 0.01) nm. The line positions in the images at the halfway point, and other spot-checked positions were all within the measurement uncertainty of their expected positions, based on the end line positions and the calculated pitch, giving good confidence that the line count was correct; a miscount of one, for example, would predict a space at the location of the middle line. The predictability of the spot-checked lines also gives confidence in the overall uniformity of the grating pitch. The source of the discrepancy between the measured and expected values, which is outside the uncertainty bounds, is still under investigation. Potential candidates include a misestimate of the temperature of the grating during fabrication, or a misestimate of the Abbe error during measurement.

Grating measurements have also alternatively been done in a single trace mode, where instead of taking a long, composite image, only a single continuous line scan is done across the sample, in the manner of a profilometer. For this mode, the coarse motion carriage alone is used to scan across the grating sample. In a typical example, we acquired a 10 mm profile in three days, working at an average speed of 50 nm s^{-1}. We have a proclivity towards slow scan rates during metrology runs to protect the probe tip from incidental contact with the surface, but this was not an optimized speed setting, and significantly faster scan rates can likely be supported without loss of accuracy or resolution. Images were taken at both ends of the single line trace both before and after the scan to verify the integrity of the tip and to check for drift and repeatability. As before, the average pitch is calculated as the total distance between end lines divided by the number of spacings, with consistency checks.

In all of our measurements of one-dimensional line gratings, we have not only taken images and data across the lines as described, but we have also taken series of images along the lines to establish the orientation of the grating with respect to the horizontal metrology axes for making alignment corrections to the pitch measurements.

Additional validation of the metrology system has been done, beyond the LFAD Cr grating, through intercomparison with the NIST line scale interferometer [23]. The vehicle for this comparison was a prototype NIST Standard Reference Material 2800. In this case, the distance between individual features was compared over a 10 mm span, and the measurements were within the estimated relative uncertainty bounds of 2×10^{-5}, $k = 2$.

3.2. High resolution

Clearly one of the motivations for developing a metrology instrument with atomic resolution is to begin to explore the use of atomic crystal lattices as intrinsic length standards, and to validate the measurement system by comparison to these. Lacking true ultra-high vacuum and versatile sample preparation facilities in M^3, one of the simplest samples to prepare and easiest to image with atomic resolution is graphite. STM images of graphite typically show a trigonal pattern with a nearest neighbour spacing of 0.25 nm. This imaging has been done also with M^3 with the scan stages in open-loop mode. Our closed-loop positioning control has some noise at the few tenths of nanometres level and at relatively low bandwidth due in part to what we believe to be a second-order effect caused by laser pointing instability due to turbulence. In order to decrease this source of noise in the interferometer measurements, we are currently developing a system for delivering the laser beams to the in-vacuum interferometer using fibre optics. In the meantime, we needed a crystal with a bigger lattice constant to begin this work.

The sample we found to use was the organic compound $(TEET)[Ni(dmit)_2]_2$, full chemical name tetra-ethyl-bis (ethylenedithio) tetrathiafulvalene-bis (nickel-bis(4, 5-dithiolato-1, 3-dithiole-2-thione)). In its crystalline form, it is an air-stable, layered semiconductor with room temperature conductivity of 1.56×10^{-2} S cm^{-1}. The crystal structure, from x-ray crystallography, is triclinic, with lattice

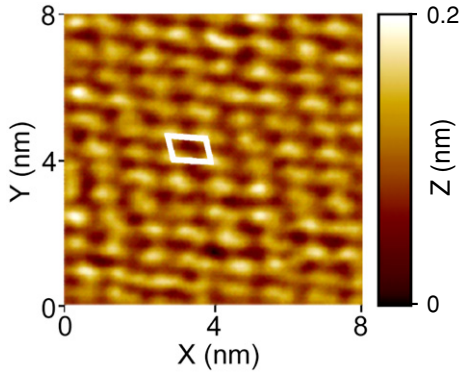

Figure 5. M^3 closed-loop metrology image of organic conducting crystal, (TEET)[Ni(dmit)$_2$]$_2$. The unit cell parameters were measured as $a = (0.70 \pm 0.01)$ nm, $b = (1.09 \pm 0.06)$ nm, and $\gamma = 106^\circ \pm 3^\circ$.

constants $a = 0.7509$ nm, $b = 1.0199$ nm, $c = 1.7097$ nm, $\alpha = 101.60^\circ$, $\beta = 93.28^\circ$ and $\gamma = 105.48^\circ$. The lattice vectors a and b are the ones accessible at the cleavage plane, and the single-layer step height is 1.6632 nm. The three to four-fold increase in the surface lattice constant relative to graphite is enough to permit the observation of the lattice using M^3, on a good day, even when operating in the noisier closed-loop control mode, as seen in figure 5.

The lattice constants that were measured for (TEET)[Ni(dmit)$_2$]$_2$ using M^3 were $a = (0.70 \pm 0.01)$ nm, $b = (1.09 \pm 0.06)$ nm, and $\gamma = 106^\circ \pm 3^\circ$, where the uncertainties quoted are one standard deviation statistical only, and do not include any estimate of systematic effects. The difference between the x-ray lattice constants and the M^3 measured values can be completely accounted for by appealing to the periodic nonlinearity commonly seen in polarization-encoded heterodyne interferometers [24]. We have previously measured the magnitude of this cyclical error for M^3 to be about 1 nm peak to peak at the optical fringe period of $\lambda/8$, or about 80 nm. For a large enough statistical sample of lattice constant measurements, randomly distributed within the optical fringe, the lengthening and foreshortening of short-distance measurements caused by this effect should average out, leaving only an increased uncertainty. Better, we also expect that in the controlled temperature and high-vacuum environment of M^3, the periodic nonlinearity should reproducibly correlate with absolute position, and therefore be mappable and correctable.

4. Nanolithography for calibration standards

Having accurate, closed-loop position control opens the possibility of creating artefacts with accurately placed features. Several methods have been used to modify surfaces on the nanometre scale with SPM tips [25]. It is not our purpose to develop new nanolithography techniques, but to use what has already been developed, in combination with the M^3 metrology system, to create artefacts with unique properties that can be used as calibration standards or special test samples. The uniqueness would lie in the accuracy of the feature placement over a relatively large area, and the small size of the calibration or test feature possible.

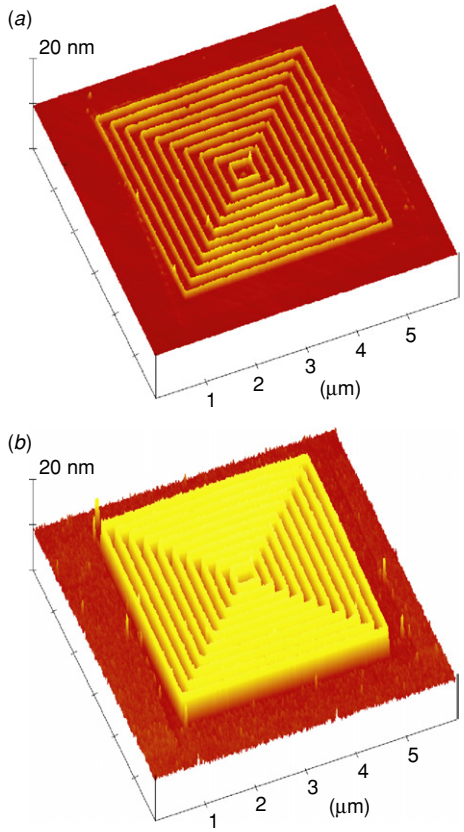

Figure 6. Pattern written by SPO lithography, using M^3's accurately guided tip. (*a*) Before etching, line height about 3 nm. (*b*) After etching, line height about 20 nm. The linewidth in this example is less than 100 nm.

We have been using scanned probe oxidation lithography (SPO) [26], to explore the possible pathways for producing artefacts. An example [27] is shown in figure 6(*a*). Here, a hydrogen terminated Si(111) surface was produced by careful wet chemical etching. The sample was loaded into the M^3 vacuum system, and the pattern written by scanning at a raised sample bias. Subsequently, the sample was removed and the test features measured using an AFM. The narrow 20 nm width of the features is attractive because it allows the possibility of producing very small pitch calibration gratings, as well as few-nanometre dimension test artefacts for the development of other metrology techniques. The height of these features as written, however, may make it difficult for other techniques to access them. Therefore, we have begun exploring the properties of these lines as etch masks for reactive ion etching (RIE), and determining appropriate RIE parameters. From the 3 nm high SPO generated lines, at least 20 nm relief can be produced by RIE (figure 6(*b*)). Our writing speed is far too slow to produce calibration artefacts for distribution by individual direct write. We are therefore considering nano-imprint lithography [28] as a possible means of replication, once the dimensional fidelity of the replication process is established. The ability, with the self same interferometer-guided probe, to both image the atomic lattice and to write larger nanometre-size features that are accessible by non-SPM techniques makes this an interesting potential route

to producing practical calibration standards that are based on the atomic lattice.

5. Conclusions

Accurate nanometre-resolution dimensional metrology over technologically significant distances is an infrastructural technology that we expect will be crucial for the continued growth of nanomanufacturing. The Molecular Measuring Machine is an instrument that we are developing at NIST to address this need. We envision dissemination of this measurement capability through the calibration of suitable transfer artefacts. These could be provided by industry or developed in-house. Especially attractive are calibration standards where the dimensions are inherently based on a physical property such as a crystal lattice constant.

Acknowledgments

This paper is a summary of work undertaken over many years at NIST; as such, there are far too many contributors to mention each by name. Especially noted are E C Teague, who initiated the project and led the early development; F E Scire for mechanical design; W B Penzes for electronics design; J S Villarrubia and J S Jun for controller and probe design; G M Witzgall, H Zhou, J Fu and R M Silver for nanolithography. We also benefitted from the help of many guest researchers from various institutions and countries; several were from Taiwan, both from the Precision Instrument Development Center and from the Industrial Technology Research Institute, Center for Measurement Science. Special thanks to A Kini from Argonne National Laboratory for providing the (TEET)[Ni(dmit$_2$]$_2$ sample and crystallographic data.

References

[1] Baller M K *et al* 2000 A cantilever array-based artificial nose *Ultramicroscopy* **82** 1–9

[2] Heath J R and Ratner M A 2003 Molecular electronics *Phys. Today* (May) 43–49
Joachim C, Gimzewski J K and Aviram A 2000 Electronics using hybrid-molecular and mono-molecular devices *Nature* **408** 541–8

[3] Craighead H G 2003 Nanostructure science and technology: impact and prospects for biology *J. Vac. Sci. Technol.* A **21** S216–21

[4] Rashba E and Gamota D 2003 Anticipatory standards and the commercialization of nanotechnology *J. Nanoparticle Res.* **5** 401–7

[5] Teague E C 1989 The National Institute of Standards and Technology molecular measuring machine project: metrology and precision engineering design *J. Vac. Sci. Technol.* B **7** 1898–902

[6] Kramar J, Amatucci E, Gilsinn D, Jun J-S, Penzes W and Scire F 1999 Toward nanometer accuracy measurements *Proc. SPIE* **36** 1017–28

[7] Kramar J A, Jun J, Penzes W B, Scheuerman V P, Scire F E and Teague E C 2001 Molecular Measuring Machine design and performance *Proc. Am. Soc. Precis. Eng.* **25** 19–22

[8] Meli F and Thalmann R 1998 Long-range AFM profiler used for accurate pitch measurements *Meas. Sci. Technol.* **9** 1087–92

[9] Bienias M, Gao S, Hasche K, Seemann R and Thiele K 1998 A metrological scanning force microscope used for coating thickness and other topographical measurements *Appl. Phys.* A **66** S837–42

[10] Schneir J, McWaid T H, Alexander J and Wilfley B P 1994 Design of an atomic force microscope with interferometric position control *J. Vac. Sci. Technol.* B **12** 3561–6

[11] Gonda S, Doi T, Kurosawa T, Tanimura Y, Hisata N, Yamagishi T, Fujimoto H and Yukawa H 1999 Real-time, interferometrically measuring atomic force microscope for direct calibration of standards *Rev. Sci. Instrum.* **70** 3362–8
Misumi I, Gonda S, Kurosawa T and Takamasu K 2003 Uncertainty in pitch measurements of one-dimensional grating standards using a nanometrological atomic force microscope *Meas. Sci. Technol.* **14** 463–71

[12] Picotto G B and Pisani M 2001 A sample scanning system with nanometric accuracy for quantitative SPM measurements *Ultramicroscopy* **86** 247–54

[13] Leach R K, Haycocks J, Jackson K, Lewis A, Oldfield S and Yacoot A 2001 Advances in traceable nanometrology at the National Physical Laboratory *Nanotechnology* **12** R1–6

[14] Breil R *et al* 2002 Intercomparison of scanning probe microscopes *Precis. Eng.* **26** 296–305

[15] Holmes M, Hocken R and Trumper D 2000 The long-range scanning stage: a novel platform for scanned-probe microscopy *Precis. Eng.* **24** 191–209

[16] Nano Positioning and Nano Measuring Machine, SIOS Messtechnik, GmbH, http://www.sios.de

[17] Dai G, Jung L, Pohlenz F, Danzerbrink H-U, Krueger-Sehm R, Hasche K and Wilkening G 2004 Measurement of micro-roughness using a metrological large range scanning force microscope *Meas. Sci. Technol.* **15** 2039–46

[18] Günther P, Fischer U C and Dransfeld K 1989 Scanning near-field acoustic microscopy *Appl. Phys.* B **48** 89–92
Giessibl F J 2000 Atomic resolution on Si(111)-(7×7) by noncontact atomic force microscopy with a force sensor based on a quartz tuning fork *Appl. Phys. Lett.* **76** 1470–2

[19] Whipple R S 1921 The design and construction of scientific instruments *Trans. Opt. Soc., Lond.* **22** 35–52

[20] Lan K-J, Yen J-Y and Kramar J A 2004 Active vibration isolation for a long range scanning tunneling microscope *Asian J. Control* **6** 179–86
Lan K-J, Yen J-Y and Kramar J A 2004 Sliding mode control for active vibration isolation of a long range scanning tunneling microscope *Rev. Sci. Instrum.* **75** 4367–73

[21] Advanced Measurement Laboratory 2004 http://www.nist.gov/public_affairs/amlbrochure.htm
The National Institute of Standards and Technology Advanced Measurement Laboratory, Gaithersburg, MD http://www.nanobuildings.com/projects/nist/

[22] McClelland J J, Scholten R E, Palm E C and Celotta R J 1993 Laser-focused atomic deposition *Science* **262** 877–80
McClelland J J, Anderson W R, Bradley C C, Walkiewicz M, Celotta R J, Jurdik E and Deslattes R D 2003 Accuracy of nanoscale pitch standards fabricated by laser-focused atomic deposition *J. Res. NIST* **108** 99–113

[23] Beers J S and Penzes W B 1999 The NIST length scale interferometer *J. Res. NIST* **104** 225–52
Beers J S and Penzes W B 2000 The NIST length scale interferometer *J. Res. NIST* **105** 779 (erratum)

[24] Bobroff N 1987 Residual errors in laser interferometry from air turbulence and nonlinearity *Appl. Opt.* **26** 2676–82
Stone J A and Howard L P 1998 A simple technique for observing periodic nonlinearities in Michelson interferometers *Precis. Eng.* **22** 220–32

[25] Zhang L B, Shi J X, Yuan J L, Ji S M and Chang M 2004 The advancement of SPM-based nanolithography *Mater. Sci. Forum* **471–472** 353–7
Marrian C R K and Tennant D M 2003 Nanofabrication *J. Vac. Sci. Technol.* A **21** S207–15

[26] Dagata J A, Schneir J, Harary H H, Evans C J, Postek M T and Bennett J 1990 Modification of hydrogen-passivated silicon

by a scanning tunneling microscope operating in air *Appl. Phys. Lett.* **56** 2001–3

[27] Zhou H, Witzgall G, Fu J, Kramar J, Hajdaj R and Silver R 2005 Reative ion etching of scanning tunneling microscope induced modification of hydrogen terminated silicon(111), in preparation

[28] Chou S Y, Krauss P R and Renstrom P J 1995 Imprint of sub-25 nm vias and trenches in polymers *Appl. Phys. Lett.* **67** 3114–6

Zankovych S, Hoffmann T, Seekamp J, Bruch J-U and Sotomayor Torres C M 2001 Nanoimprint lithography: challenges and prospects *Nanotechnology* **12** 91–5